Electronic Supplementary Material (ESI) for Nanoscale.

Supplementary Information:

Unconventional Inner-TL Electric Polarization in TL-$LaOBiS_2$ with Ultrahigh Carrier Mobility

*Chao He[a], Jiajun Zhu[a], Yong-Hong Zhao[a], Chang Liu[b] and Botao Fu[a]**

a. College of Physics and Electronic Engineering, Center for Computational Sciences, Sichuan Normal University, Chengdu, 610068, China.

b. Institute for Computational Materials Science, School of Physics and Electronics, Henan University, Kaifeng 475004, China.

1. Structure stability of T2 and T3 TL-$LaOBiS_2$

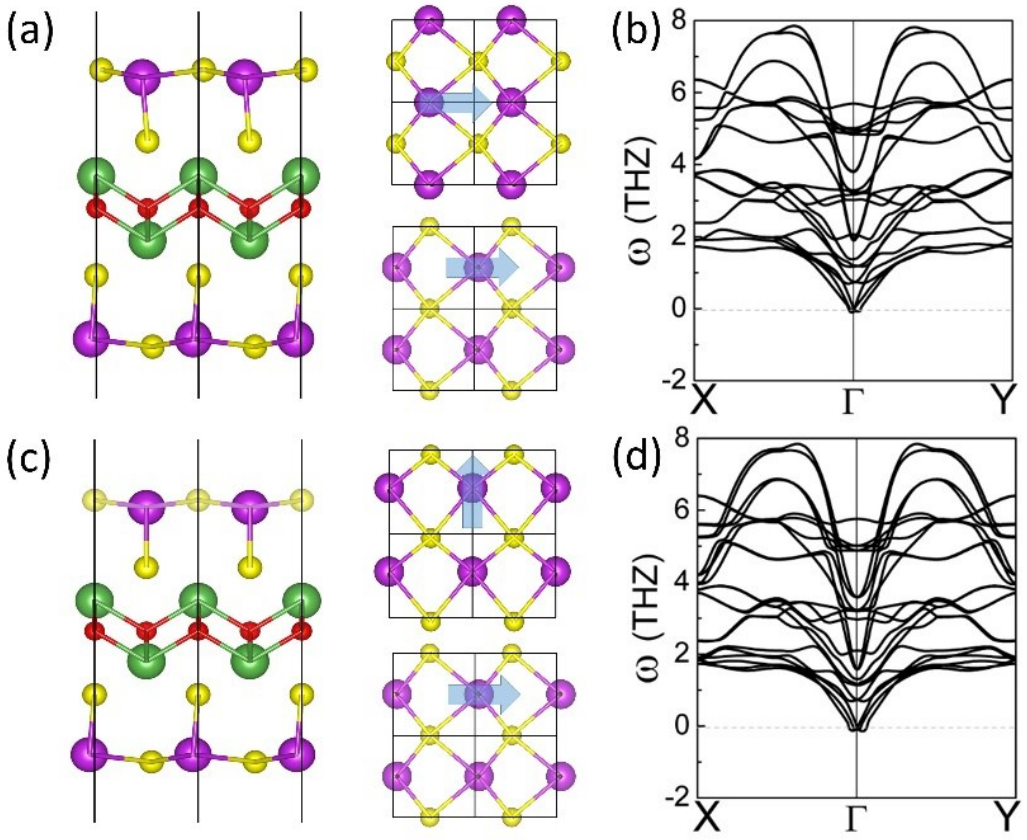

Figure S1 The geometric structures and phonon spectra of T2 and T3 TL-$LaOBiS_2$. (a) The geometric structures of T2 TL-$LaOBiS_2$, the arrow indicates the parallel polarization on top and bottom BiS_2 layers. (c) The geometric structures of T3 TL-$LaOBiS_2$, the arrow indicates the orthogonal polarization on top and bottom BiS_2 layers. (b) and (d) are the phonon spectra of T2 and T3 phases, respectively. There is no negative frequency for both T2 and T3 phases, which indicates the dynamic stability of them.

2. Details for the calculation of Curie temperature based on Monte Carlo method.

We employed the Landau phase transition theory which takes the electric polarization P as the order parameter. The free energy of system F can be expanded in terms of the polarization as following:

$$F = \sum_i (\frac{A}{2} P_i^2 + \frac{B}{4} P_i^4 + \frac{C}{6} P_i^6) + \sum_{<i,j>} (P_i - P_j)^2 \qquad (S1)$$

Where P_i is the polarization of each unit cell, <i, j> denotes the nearest neighbors. As we use the mean-field approximation, only the nearest neighbor is taken into consideration. The first three terms describe the energy contribution from the local polarization up to sixth order. The last term captures the coupling between the nearest polarizations, which associates with the two-dimension geometrical characteristic and plays a crucial for the polarization ordering and the phase transition. After we obtained the values of those parameters by fitting DFT results with model S1, we can use Monte Carlo simulations to investigate the temperature impact on this model and thus obtain the phase transition temperature T_c. For TL-$LaOBiS_2$, the fitted values of four parameters in formula S1 are $A=-12.366\times10^{-2}$, $B=3.489\times10^{-4}$, $C=0.005\times10^{-6}$, D=0.155. Here the unit of P_i is $\mu C/cm^2$ and the unit of F is meV. The temperature dependent polarization is demonstrated in figure 4(c) and the ferroelectric phase is stable below the transition temperature around 420 K.

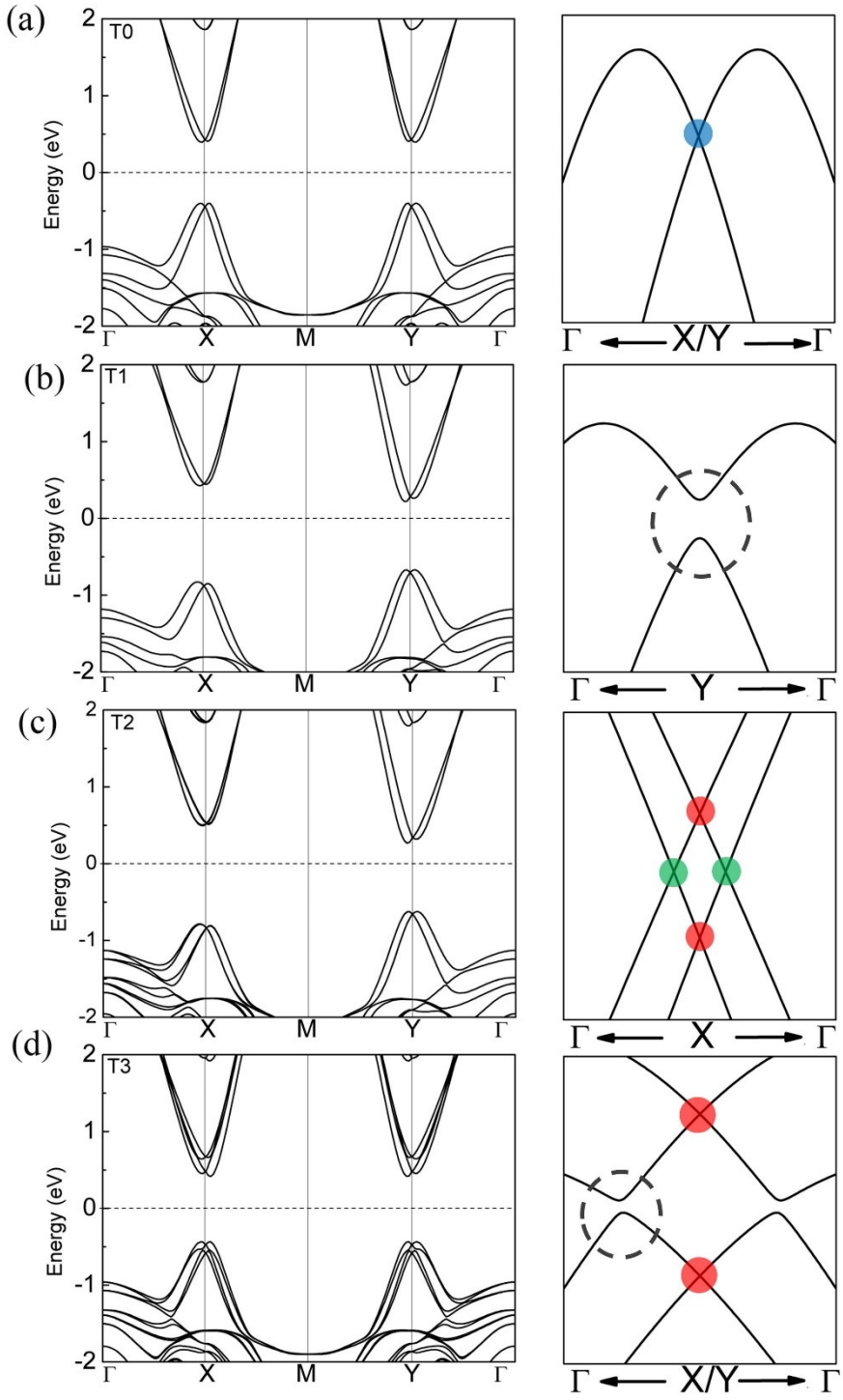

Figure S2 (a)-(d) The left side are the band structures of TL-LaoBiS_2 under HSE+SOC correction, the right side are enlarged views near VBM at X or Y point. The red circle indicates WPs at X/Y point while the green circle indicates WPs along XΓ path. The blue circle indicates the Dirac points at X/Y point. For T0 phase, four-fold degenerate 2D Dirac points (blue circle) emerge at both X and Y points, which are protected by $\hat{C}_{2x}$ and $\hat{C}_{2y}$ respectively. For T1 phase, the Dirac cone at X is remain because of $\hat{C}_{2y}$, but at Y point is opened (highlighted inside the dashed circle). For T2 phase with breaking inversion symmetry, the Dirac point at X point splits into two pairs of Weyl points, one (red circle) locate at X point protected by the time reverse symmetry, the other (green circle) locate along XΓ protected by the slide mirror $\hat{M}_{y}$. For T3 case with lowest symmetry, the Weyl points along XΓ are gapped while the Weyl points (red circle) at X/Y point are untouched.

3. Band structure with HSE+SOC correction.

4. Mobility of T0 TL-$LaOBiS_2$

On the basis of the effective mass approximation and the deformation potential theory, the carrier mobility of T0-T3 TL-$LaOBiS_2$ are calculated from following formula:

$$\mu_{2D\_x,y} = \frac{e\hbar^3 C_{2D\_x,y}}{k_B T m^*_{x,y} \sqrt{m^*_x m^*_y} (E^{\,i}_{x,y})^2}$$

The $m^*_{x,y}$ is the effective mass in transport direction, the $C_{2D\_x,y}$ is the 2D elastic modulus, the $E^{\,i}_{x,y}$ is the deformation potential constant for the ith band. The subscript x and y represent corresponding transport directions. The temperature T is set to 300 K. The $m^*_{x,y}$ can be directly estimated from the band structure by $m^* = \hbar^2(\partial^2 E/\partial^2 k)^{-1}$. The elastic modulus is derived from $(E - E_0)/S_0 = C_{2D}\left(\Delta l/l_0\right)^2/2$. The deformation potential E^i can be derived from $\Delta E = E^i/(\Delta l/l_0)$, ΔE is the energy shift at the CBM (for electron) or VBM (for hole) respect to an infinitesimal strain.

Table S1. The effective mass m^*_x (m^*_y), deformation potential $E_x(E_y)$, elastic modulus C_{2D_x}(C_{2D_y}) and carrier mobility μ_{x_2D} (μ_{y_2D}) are listed for T0-T3 TL-$LaOBiS_2$. The subscript x and y represent x and y direction. The "e" and "h" on the first column refer to ''electron'' and "hole", respectively.

T0	m^*_x/m_0	m^*_y/m_0	E_x (eV)	E_y (eV)	C_{2D_x} (Jm^{-2})	C_{2D_y} (Jm^{-2})	μ_{2D_x} ($10^3 cm^2V^{-1}s^{-1}$)	μ_{2D_y} ($10^3 cm^2V^{-1}s^{-1}$)
e	0.14	0.19	9.94	2.22	169.56	169.56	1.57	23.20
h	0.23	0.27	8.29	2.47	169.56	169.56	0.90	8.63

T1	m^*_x/m_0	m^*_y/m_0	E_x (eV)	E_y (eV)	C_{2D_x} (Jm^{-2})	C_{2D_y} (Jm^{-2})	μ_{2D_x} ($10^3 cm^2V^{-1}s^{-1}$)	μ_{2D_y} ($10^3 cm^2V^{-1}s^{-1}$)
e	0.16	0.15	9.70	1.57	163.81	124.81	1.47	45.54
h	0.25	0.16	8.15	2.02	163.81	124.81	1.03	19.98

T2	m^*_x/m_0	m^*_y/m_0	E_x (eV)	E_y (eV)	C_{2D_x} (Jm^{-2})	C_{2D_y} (Jm^{-2})	μ_{2D_x} ($10^3 cm^2V^{-1}s^{-1}$)	μ_{2D_y} ($10^3 cm^2V^{-1}s^{-1}$)
e	0.16	0.21	9.55	1.58	162.42	123.39	1.27	26.84
h	0.26	0.31	8.07	2.00	162.42	123.39	0.71	7.33

T3	m^*_x/m_0	m^*_y/m_0	E_x (eV)	E_y (eV)	C_{2D_x} (Jm^{-2})	C_{2D_y} (Jm^{-2})	μ_{2D_x} ($10^3 cm^2V^{-1}s^{-1}$)	μ_{2D_y} ($10^3 cm^2V^{-1}s^{-1}$)
e	0.16	0.20	9.55	1.63	144.67	144.25	1.14	31.72
h	0.25	0.30	8.07	2.18	144.67	144.25	0.66	7.72

5. Ferroelectric origin of TL-$LaOBiS_2$ and its analogues.

Table S2. The optimized lattice constants (**a**, **b**), the exfoliation energies (E_{cl}) from their bulk crystals, the ferroelectric structural distortion strength defined as: L2-L1, the polarization strength (P_s), the transition barrier (E_b) , and the lattice mismatch (L_m) of five tripe-layer materials with same structure as TL-$LaOBiS_2$.

	a (Å)	**b** (Å)	E_{cl} (J/m^2)	L2-L1 (Å)	P_s ($\mu C/cm^2$)	E_b (meV)	L_m (Å)
$LaOBiS_2$	4.022	4.029	1.022	0.280	17.410	6.5	0.297
$LaOBiSe_2$	4.108	4.117	0.301	0.142	16.359	0.7	0.192
$LaOSbS_2$	3.989	4.071	0.284	0.528	22.254	102.3	0.482
$LaOSbSe_2$	4.078	4.128	0.282	0.424	31.072	52.7	0.280
$SrFBiS_2$	4.030	4.058	3.408	0.264	16.045	7.3	0.238

It is known that the ferroelectric mechanism involves cations (e.g. Sb^{3+} and Bi^{3+}) with "lone pair" electrons which have a formal ns^2 valence electron configuration. It is proposed in Ref. 86 that the hybridization between the localized ns^2 states and a low-lying ns^1np^1 excited state tends to form displacive distortions. If the lowering in energy associated with this hybridization interaction is larger than the interionic repulsion opposing the ion shift, then a ferroelectric distortion emerges. This means the emergent of ferroelectricity involves two aspects. One is the existence of cations containing "lone pair" electrons, namely intrinsic mechanism. The other is proper lattice constant under which the ion shift is energy favorable, namely, external mechanism. The latter can be largely influence by external strain or lattice mismatch.

Appling this theory to TL-$LaOBiS_2$, we find the "lone pair" electrons indeed exist in Bi^{3+} of BiS_2 layer, while no "lone pair" electrons on La^{3+} of LaO layer. This explains that why BiS_2 layer becomes obviously polar but LaO layer remain un-polar in TL-$LaOBiS_2$. In fact, whether the ferroelectric distortion can happen on BiS_2 layer not only depends on the "lone pair" electrons on Bi^{3+} but also relies on the lattice constant. Because the interionic repulsion effect that oppose the ion polarization can be effectively tuned by the lattice constant. Specifically, due to the unique sandwiched structure of TL-$LaOBiS_2$, the impact from lattice constant can be greatly tuned by the lattice mismatch between LaO and BiS_2 layers. To clearly demonstrate this lattice mismatch effect, taking TL-$LaOBiS_2$ for instance, we calculate optimized lattice constant of independent BiS_2 and LaO layers separated from TL-$LaOBiS_2$, which are 3.819 Å and 4.116 Å respectively. The lattice mismatch (L_m) is defined by LaO's lattice constant minus BiS2's, which is 0.297 Å for TL-$LaOBiS_2$. We can see the lattice constant of LaO is larger than that of BiS_2, which implies that in the TL-$LaOBiS_2$ the BiS_2 layer bears tensive strain compare with its free states, which is beneficial for the in-plane polarization. Similarly, we further calculate the lattice mismatch for ferroelectric materials listed in last column of table S2. We discover that except $LaOSbSe_2$ and $SrFBiS_2$ the other three materials perfectly satisfy our previous assumption that the polarization is almost positively related with lattice mismatch. Therefore, we conclude that the emergent polarization on BiS_2 layer of TL-$LaOBiS_2$ originating from the from "lone pairs" electrons of Bi^{3+} and can be induced by the lattice misfit effect between LaO and BiS_2 layers.